Charged defects in two-dimensional semiconductors of arbitrary thickness and geometry: Formulation and application to few-layer black phosphorus

Dan Wang,[1] Dong Han,[2] Xian-Bin Li,[1,3,*] Nian-Ke Chen,[1] Damien West,[3,†]
Vincent Meunier,[3] Shengbai Zhang,[1,3] and Hong-Bo Sun[1]

[1]*State Key Laboratory on Integrated Optoelectronics, College of Electronic Science and Engineering, Jilin University, Changchun 130012, China*

[2]*State Key Laboratory of Luminescence and Applications, Changchun Institute of Optics, Fine Mechanics and Physics, Chinese Academy of Sciences, Changchun 130033, China*

[3]*Department of Physics, Applied Physics, and Astronomy, Rensselaer Polytechnic Institute, Troy, New York 12180, USA*

(Received 14 March 2017; revised manuscript received 30 August 2017; published 9 October 2017)

Energy evaluation of charged defects is tremendously important in two-dimensional (2D) semiconductors for the industrialization of 2D electronic devices because of its close relation with the corresponding type of conductivity and its strength. Although the method to calculate the energy of charged defects in single-layer one-atom-thick systems of equilateral unit-cell geometry has recently been proposed, few-layer 2D semiconductors are more common in device applications. As it turns out, one may not apply the one-layer formalism to multilayer cases without jeopardizing accuracy. Here, we generalize the approach to 2D systems of arbitrary cell geometry and thickness and use few-layer black phosphorus to illustrate how defect properties, mainly group-VI substitutional impurities, are affected. Within the framework of density functional theory, we show that substitutional Te (Te_P) is the best candidate for *n*-type doping, and as the thickness increases, the ionization energy is found to decrease monotonically from 0.67 eV (monolayer) to 0.47 eV (bilayer) and further to 0.33 eV (trilayer). Although these results show the ineffectiveness of the dielectric screening at the monolayer limit, they also show how it evolves with increasing thickness whereby setting a new direction for the design of 2D electronics. The proposed method here is generally suitable to all the 2D materials regardless of their thickness and geometry.

DOI: 10.1103/PhysRevB.96.155424

I. INTRODUCTION

Two-dimensional (2D) materials are promising candidates for future high-performance electronics and optoelectronics due to their intriguing properties [1–8]. One of the prerequisites for achieving this goal is to understand the properties of the defect. This is not only because native defects and unintentional impurities are usually unavoidable in a real sample and can strongly affect the physical properties of materials, but also because intentional doping is a primary means to control *n*- or *p*-type conductivity, which is a key ingredient for the design of optoelectronic devices [9–12]. This has prompted the theoretical development of methods to study ionization energies (IEs) or charged energies of defects in monolayer (ML) materials to overcome the drawback of energy divergence accompanied with the use of a conventional *jellium* approach [13,14]. Due to reduced dimensionality and screening, defects usually introduce deep (i.e., close to midgap) levels in such materials [13,15,16]. However, the levels are found to be shallower when the monolayer material is placed in a dielectric environment, such as on a substrate, which can strongly screen the Coulomb interaction between charges [15]. This suggests that controllable electrical conductivity should be easier to obtain in few-layer systems. Moreover, few-layer 2D materials or a monolayer on a substrate is more practical in electronic devices instead of a freestanding monolayer [5,17–22]. Therefore, understanding defects in few-layer 2D materials is a significant goal for the fundamental understanding of low-dimensional electronics. One possibility to tackle the physics of defects in multilayer could be the use of a supercell with extremely large vacuum size to mimic that the few layer is still thin enough compared to this vacuum size and the application of the existing monolayer formalism [13]. However, such calculations are usually prohibitive due to the associated computational cost. Thus, it is essential to update the formalism of IEs of defects in 2D materials for systems with more than one layer under the condition of limited vacuum size.

In this paper, we derive a general formalism of charged energies based on Ref. [13] for not only one-atom-thick systems of unilateral geometry, such as hexagonal boron nitride, but also 2D systems of arbitrary thickness and geometry including one-molecule-thickness [such as MoS_2 and black phosphorus (BP)], few-layer-thick 2D systems on a substrate, as well as surfaces and interfaces. We apply this approach to calculate the IEs of the phosphorus vacancy (V_P) and substitutional group-VI impurities (O_P, S_P, Se_P, and Te_P) in BP from monolayer up to trilayer (3L). Due to the increased screening in thick layers, the IE of Te_P is reduced from 0.67 eV for ML BP to 0.47 eV for bilayer [(2L) BP] and to 0.33 eV for trilayer 3L BP. The results show that shallow dopants are more practical and easier to obtain in few-layer BP and most likely in other few-layer 2D semiconductors as well.

II. METHOD AND FORMULATION

The calculations were performed using density functional theory [23,24] with the Perdew-Burke-Ernzerhof

*lixianbin@jlu.edu.cn
†westd2@rpi.edu

approximation for the exchange-correlation functional [25] as implemented in the Vienna *ab initio* simulation package (VASP) [26,27]. Note that, although advanced functionals could yield more accurate results [28,29], the methodology developed here is independent of the choice of functionals. The cutoff energy for the plane-wave basis was 520 eV. The $3 \times 2 \times 1$ Monkhorst-Pack mesh grid was used for k-point sampling, and spin polarization was included. All atoms were relaxed until the Hellman-Feynman forces on individual atoms are less than 0.02 eV/Å. For charged defects, a homogenous countercharge (i.e., the *jellium* background) was used to maintain charge neutrality [9,30,31].

The formation energy of a defect α of charge q is given by [32]

$$\Delta H_f(q,d) = E(q,d) - E(\text{host}) + \sum_i n_i\mu_i + q(\varepsilon_{\text{VBM}} + \varepsilon_F)$$
$$= \Delta E(q,d) + \sum_i n_i\mu_i + q(\varepsilon_{\text{VBM}} + \varepsilon_F), \quad (1)$$

where $\Delta E(q,d)$ is the total energy difference between the supercell with defect d, $E(q,d)$ and the perfect supercell $E(\text{host})$, n_i is the number of atoms exchanged when the defect is created, μ_i is the chemical potential of each of the atoms exchanged, and ε_F is the Fermi energy with respect to the valence-band maximum (VBM) of the host material ε_{VBM}. The defect transition energy is defined by the Fermi energy at which two different charge states (q' and q) of the same defect d have the same formation energy $\Delta H_f(q,d) = \Delta H_f(q',d)$. Namely,

$$\varepsilon(q/q') + \varepsilon_{\text{VBM}} = [\Delta E(q,d) - \Delta E(q',d)]/(q' - q). \quad (2)$$

A donor ionization energy, which evaluates the ability of the defect to produce free carriers, is defined by $\varepsilon(+/0)$ with respect to the conduction-band minimum (CBM) ε_{CBM}, whereas an acceptor ionization energy is defined by $\varepsilon(0/-)$ with respect to the VBM.

The scheme leads to an energy error of $\delta E \propto 1/\sqrt[3]{V}$ for 3D materials, which means gradually converged energies with increasing cell size but encounters a divergence with increasing vacuum size for charged defects for 2D materials [13,14]. The divergence originates from the long-range Coulomb interaction between the charged defects and the compensating *jellium* charge. This difficulty is resolved by an extrapolation of the asymptotic IE expression provided in Ref. [13],

$$\text{IE}(S,L_Z) = \text{IE}_0 + \frac{\alpha}{\sqrt{S}} + \frac{q^2}{24S\varepsilon_0}L_Z$$
$$= \text{IE}_0 + \frac{\alpha'}{L_s} + \frac{q^2}{24L_s^2\varepsilon_0 \sin\theta}L_Z, \quad (3)$$

where IE_0 is the converged (converged with respect to variable cell size) ionization energy and L_s is the in-plane equilateral cell size, i.e., $L_s = L_x = L_y$, $S = L_s^2 \sin\theta$ is the surface area with θ being the angle between L_x and L_y, and L_Z is the vertical cell size. This method has been shown to work well for defects in monolayer boron nitride [13]. However, direct application of Eq. (3) does not adequately describe the asymptotic behavior of two-dimensional systems with certain thicknesses, such as 3L BP studied here.

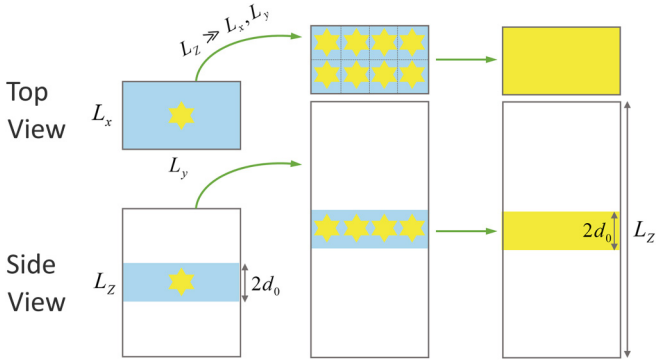

FIG. 1. A schematic of the asymptotic limits of a charged defect (yellow star) in a 2D system (light blue) with thickness ($2d_0$) and nonequilateral unit-cell geometry ($L_x \neq L_y$) for the limit of $L_Z \gg L_x, L_y$.

Equation (3) is derived in Ref. [13] from a formal expansion of the calculated ionization energy in a power series of L_x ($L_y = \gamma L_x$) and L_Z, namely (for a more general expression, L_s is replaced by L_x here),

$$\text{IE}(L_x,L_Z) = \sum_{i,j=-\infty}^{\infty} c_{i,j}L_x^i L_Z^j. \quad (4)$$

By taking three separate physical limits: (1) L_x and L_y are fixed, $L_Z \to \infty$; (2) L_Z is fixed, L_x and $L_y \to \infty$; and (3) L_x, L_y, and $L_Z \to \infty$, the power expansion can be reduced substantially to

$$\text{IE}(L_x,L_Z) = \cdots + \frac{1}{L_Z^2}\left(\cdots + \frac{c_{-2,-2}}{L_x^2} + \frac{c_{-1,-2}}{L_x} + c_{0,-2}\right)$$
$$+ \frac{1}{L_Z}\left\{t\,\ln(L_x) + c'_{0,-1} + \frac{c'_{-1,-1}}{L_x} + \cdots\right\}$$
$$+ \left(\cdots + \frac{c_{-2,0}}{L_x^2} + \frac{c_{-1,0}}{L_x} + c_{0,0}\right)$$
$$+ L_Z\left(\frac{c_{-2,1}}{L_x^2}\right). \quad (5)$$

Equation (3) then is arrived at by requiring that $L_Z \gg L_x \gg 1$. Although the requirement that $L_Z \gg L_x$ is physically clear, it is not quite clear in which cases the largeness of L_x (or L_Z for that matter) enables the dropping of terms proportional to $\frac{1}{L_x}, \frac{1}{L_x^2}$, etc. To gain a better understanding of which terms need to be kept for practical calculations, we revisit limit (1) in the more general situation of a charged defect in a dielectric slab of finite thickness.

In this limit of $L_Z \to \infty$ at fixed L_x and $L_y = \gamma L_x$, the system can be considered as a charged slab with area S and thickness $2d_0$ in a uniform *jellium* background, see Fig. 1. One may integrate the energy density $\frac{1}{2}\boldsymbol{E}^2\varepsilon_\perp\varepsilon_0$ where $|E| = \frac{q|z|}{2S\varepsilon_\perp\varepsilon_0}(\frac{1}{d_0} - \frac{2}{L_Z})$ $(-d_0 < z < d_0)$ and $\frac{1}{2}\boldsymbol{E}^2\varepsilon_0$ where $|E| = \frac{q}{2S\varepsilon_0}(1 - \frac{2|z|}{L_Z})$ $(-\frac{L_Z}{2} < z < -d_0, d_0 < z < \frac{L_Z}{2})$ to obtain the

total electrostatic energy,

$$E_{\text{total}} = \frac{q^2}{24S\varepsilon_0}\left[(L_Z - 4d_0) - 2d_0\left(1 - \frac{1}{\varepsilon_\perp}\right)\right] + \frac{q^2 d_0^3}{3S\varepsilon_0}\left(\frac{1}{\varepsilon_\perp} - 1\right)\frac{1}{L_Z^2} + \frac{q^2 d_0^2}{4S\varepsilon_0}\left(2 - \frac{4}{3\varepsilon_\perp}\right)\frac{1}{L_Z}, \quad (6)$$

where ε_0 is the vacuum dielectric constant (i.e., the absolute dielectric constant as the relative dielectric constant of vacuum is 1) and $\varepsilon_\perp$ is the out-of-plane dielectric constant (relative dielectric constant) of the 2D material (see the Appendix for details). As $S = L_x \times L_y \times \sin\ \theta = \gamma L_x^2 \sin\ \theta$, we find

$$E_{\text{total}} = \frac{q^2}{24\gamma L_x^2 \varepsilon_0 \sin\ \theta}\left[(L_Z - 4d_0) - 2d_0\left(1 - \frac{1}{\varepsilon_\perp}\right)\right] + \frac{q^2 d_0^3}{3\gamma L_x^2 \varepsilon_0 \sin\ \theta}\left(\frac{1}{\varepsilon_\perp} - 1\right)\frac{1}{L_Z^2} + \frac{q^2 d_0^2}{4\gamma L_x^2 \varepsilon_0 \sin\ \theta}\left(2 - \frac{4}{3\varepsilon_\perp}\right)\frac{1}{L_Z}. \quad (7)$$

From this limit, the IE should be dominated by the L_Z^n term $n \in [-2,1]$. Here, we explicitly see that, as the thickness of the slab ($2d_0$) increases, the energy has greater contributions from L_Z^{-2} and L_Z^{-1} which vanish in the strictly 2D limit ($L_Z \to \infty$). Also, worth noting is the presence of term $\propto d_0/L_x^2$ in Eq. (7). Although this is an idealized system, we see that the thickness of the slab plays an important role as the appropriate physical distance to which we should compare L_x and L_Z. Hence, Eq. (3) is expected to be valid when $L_Z \gg L_x \gg d_0$.

For the case of 3L BP however, with $d_0 = 0.66$ nm (thickness $2d_0$), neglecting quadratic terms in L_x, even with a lateral dimension of 4 nm would constitute ignoring terms $\sim$120 meV in the ionization energy. Furthermore, simultaneously requiring $L_Z \gg L_x$ would drastically increase computational time. In order to obtain a tractable method for dealing with defects in this system, we include in the fitting of the ionization energy terms which are up to quadratic in length where we truncate the series as follows:

$$\text{IE}(L_x, L_Z) = \frac{c_{0,-2}}{L_Z^2} + \frac{c(L_x)}{L_Z} + \left(\frac{c_{-2,0}}{L_x^2} + \frac{c_{-1,0}}{L_x} + \text{IE}_0\right) + L_Z\left(\frac{c_{-2,1}}{L_x^2}\right), \quad (8)$$

where $c(L_x)$ contains the logarithmic divergence L_x from Eq. (5), $c(L_x) = t\ \ln(L_x) + c'_{0,-1} + \frac{c'_{-1,-1}}{L_x}$, and $\text{IE}_0 = c_{0,0}$ (as $L_x, L_Z \to \infty$, only $c_{0,0}$ survives and thus $c_{0,0}$ equals IE_0). Instead of directly fitting all parameters simultaneously in Eq. (8), we define

$$\overline{\overline{\text{IE}(L_x, L_Z)}} = \text{IE}(L_x, L_Z) - \frac{c_{0,-2}}{L_Z^2} - \frac{c(L_x)}{L_Z} - L_Z\left(\frac{c_{-2,1}}{L_x^2}\right) = \frac{c_{-2,0}}{L_x^2} + \frac{c_{-1,0}}{L_x} + \text{IE}_0. \quad (9)$$

$\overline{\overline{\text{IE}(L_x, L_Z)}}$ consists of terms of $\text{IE}(L_x, L_Z)$, L_Z^{-2}, L_Z^{-1}, and L_Z^1, and it equals the coefficient of the L_Z^0 term (right-hand side of the equation). Their specific values can be obtained by fitting calculated $\text{IE}(L_x, L_Z)$ with increasing vacuum size L_Z at different L_x's. Then IE_0 is obtained as the intercept of $\overline{\overline{\text{IE}(L_x, L_Z)}}$ at $1/L_x \to 0$. Therefore, the difficult problem of taking the limits of $L_x \to \infty$ and $L_Z \to \infty$ is transformed into a simpler problem of finding the intercept of $\overline{\overline{\text{IE}(L_x, L_Z)}}$. The results obtained using this way, denoted by method 1, are shown in Figs. 3(a)–3(c) which will be detailedly discussed below. Although this method gives consistent results, the numbers of the calculations involved are laborious, which has motivated us to investigate a more approximate method to determine the ionization energy.

In practical application, the requirement of large L_Z is much easier to obtain than that of large L_x as it only involves increasing the vacuum dimension instead of the number of atoms. If we maintain $L_Z \gg L_x$, we can drop the $\frac{1}{L_Z}$ and $\frac{1}{L_Z^2}$ terms from Eq. (8) which then reduces to

$$\text{IE}(L_x, L_Z) = \frac{c_{-2,0}}{L_x^2} + \frac{c_{-1,0}}{L_x} + \text{IE}_0 + L_Z\left(\frac{c_{-2,1}}{L_x^2}\right). \quad (10)$$

In order to obtain a more practical expression, which reduces the amount of computation required, we can approximate the value of the coefficient $c_{-2,0} = \frac{q^2}{24\gamma\varepsilon_0 \sin\ \theta}[-4d_0 - 2d_0(1 - \frac{1}{\varepsilon_\perp})]$ from the ideal case presented in Eq. (7), obtaining

$$\text{IE}(L_x, L_Z) = \frac{c_{-1,0}}{L_x} + \text{IE}_0 + \frac{q^2}{24\gamma L_x^2 \varepsilon_0 \sin\ \theta} \times \left[(L_Z - 4d_0) - 2d_0\left(1 - \frac{1}{\varepsilon_\perp}\right)\right], \quad (11)$$

which also includes the value of $c_{-2,1} = \frac{q^2}{24\gamma\varepsilon_0 \sin\ \theta}$, which is known exactly. When compared with Eq. (3) where L_Z is the vacuum size, $L'_Z = (L_Z - 4d_0) - 2d_0(1 - \frac{1}{\varepsilon_\perp})$ in Eq. (11) here may be considered as an effective vacuum size. Then IE_0 can be obtained in the same way as that proposed in Ref. [13]. Note that IE_0 obtained in this way should be a function of the threshold of L_Z, denoted by L_Z^T at which the terms of L_Z^{-2} and L_Z^{-1} are considered to be negligible, namely, $\text{IE}_0(L_Z^T)$. $\text{IE}_0(L_Z^T)$ approaches the actual one at $L_Z^T \to \infty$, so the real IE_0 can be deduced by making $1/L_Z^T \to 0$. Since the terms of L_Z^{-2} and L_Z^{-1} diverge faster and faster with increasing thickness $2d_0$ considering the ratio of $2d_0/L_Z$, L_Z^T should become larger with increasing thickness. This way to get the actual IE_0 is denoted by method 2.

Two kinds of native defects (vacancy and interstitial) and four kinds of substitutional impurities (O, S, Se, and Te) are calculated here. In addition to Te substitution, the IEs for other defects in ML BP are all obtained by Eq. (11) with $L_Z^T = 4$ nm in this paper. For Te substitution, which is adopted to explore the dielectric effect in few-layer BP, the IEs in ML BP, 2L BP, and 3L BP are all calculated using method 1 [Eq. (9)] and method 2 [Eq. (11)]. The dimensions of the supercell size are 4×4, 5×5, and 6×6 for $L_x \times L_y$, and (2–5 nm), (2.5–8 nm), and (3–8.5 nm) for L_Z in ML BP, 2L BP, and 3L BP, respectively. It should be noted that in our formulation $\gamma = L_y/L_x$ must remain unchanged during the extrapolation.

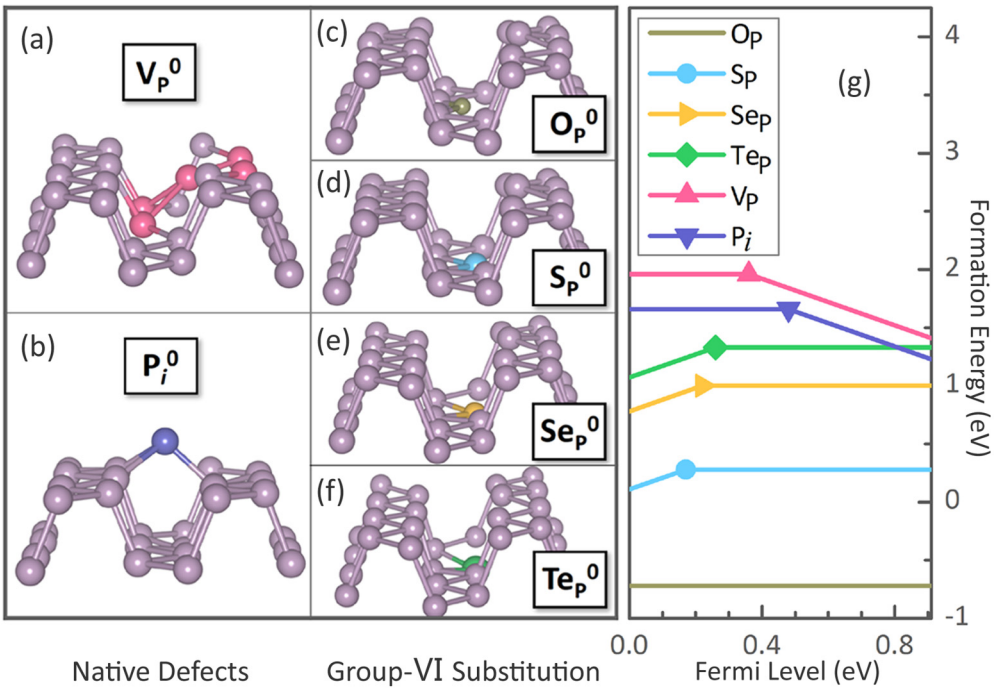

FIG. 2. (a)–(f) Optimized atomic structures of native defects V_P and P_i and substitutional group-VI impurities, O_P, S_P, Se_P, and Te_P in ML BP. (g) Their formation energy as a function of Fermi energy within the calculated generalized gradient approximation band gap of 0.91 eV. Each P atom has three nearest-neighbor (*nn*) P atoms. In (a), the out-of-plane *nn* P of the vacant P atom in the bottom layer forms chemical bonds with its two in-plane *nn* Ps. Five P atoms are relaxed significantly due to this rebonding, and they are all marked in pink. In (b)–(f), interstitial P and substitutional O, S, Se, and Te are marked in purple, tawny, light blue, yellow, and green, respectively.

III. RESULTS AND DISCUSSIONS

Figures 2(a)–2(f) show the optimized atomic structures of native defects and substitutional impurities in ML BP. Their formation energies as a function of Fermi energy are shown in Fig. 2(g). The native defects here include the phosphorus vacancy (V_P) and the interstitial (P_i). As most BPs show *p*-type conductivity in the laboratory [4,5,33–35], four substitutional group-VI elements (O_P, S_P, Se_P, and Te_P) are considered here to explore the possibility of *n*-type conductivity. For V_P, the top-layer P atom, originally bonded to the vacant P atom in the bottom layer, goes down in position to form fourfold coordination. Despite that, the formation energy of neutral V_P (=1.96 eV) is still the largest. For P_i, the foreign P atom can bond to three host P atoms, so its energy is relatively low. V_P and P_i are acceptors with deep transition energies at $\varepsilon_{VBM} + 0.36$ and $+0.48$ eV, respectively. The group-VI elements S, Se, and Te, on the other hand, favor twofold coordination, which leaves one dangling bond (DB) in the top-layer P. Hence, they are all donors. Whereas the formation energy follows the trend Te > Se > S, the donor levels at $\varepsilon_{CBM} - 0.67$, -0.69, and -0.74 eV get deeper due to the increase in localization of P DB. Oxygen is somewhat an exception as the formation energy for charge neutral O_P is negative now at -0.72 eV due to its exceptionally large electronegativity, which is reminiscent of the fact that BP is oxidized very easily by air. Due to the significantly increased localization of the P DB in O_P, the donor level also drops significantly, 0.11 eV below the VBM.

In view of the above results, the best candidate for *n*-type doping of ML BP is Te_P ($\varepsilon_{CBM} - 0.67$ eV). However, these levels are still too deep to supply a sufficient amount of carriers for electronic applications. (With a more accurate theoretical band gap, the situation is expected to only get worse since the functional used here is known to systematically underestimate the band gap [36,37].) The depth here mainly comes from the weak screening of 2D semiconductors, leading to a stronger effective Coulomb attraction between opposite charges, compared to behavior in bulk material [15]. The screening, however, should get stronger as the layer thickness increases. For the clarity of discussion and for simplicity, in our paper, defects are kept at the bottom of the first layer as in Fig. 2. Altering defect positions is expected to alter numerical results but not the conclusion.

Figures 3(a)–3(c) show the IE(L_x, L_Z) of Te_P in ML BP, 2L BP, and 3L BP, respectively. In ML BP, the IE(L_x, L_Z) is nearly in linear divergence with increasing L_Z at fixed L_x, which means that the terms of L_Z^{-2} and L_Z^{-1} do not play a major role in the energy divergence. However, they indeed do that in 2L BP and 3L BP where the energies deviate from linear divergence at small L_Z. The intercepts at $1/L_x \to 0$ of $\overline{\mathrm{IE}(L_x, L_Z)}$ denote the real ionization energies IE_0, which become shallower with increasing layer thickness: e.g., 0.67, 0.47, and 0.33 eV for ML BP, 2L BP, and 3L BP, respectively. As shown in Fig. 3(d), IE_0 also is obtained with method 2 [Eq. (11)]. In this way, the terms of L_Z^{-2} and L_Z^{-1} in Eq. (8) are ignored at L_Z^T (threshold of L_Z at which the terms of L_Z^{-2} and L_Z^{-1} are ignored), and IE_0 is dependent on L_Z^T, i.e., $IE_0(L_Z^T)$. Direct extrapolation of the linear dependence in $1/L_Z^T$ of $IE_0(L_Z^T)$ yields the actual value IE_0 [orange arrows in Fig. 3(d)] being 0.67, 0.43, and 0.37 eV for ML BP, 2L BP, and 3L BP, respectively. The results

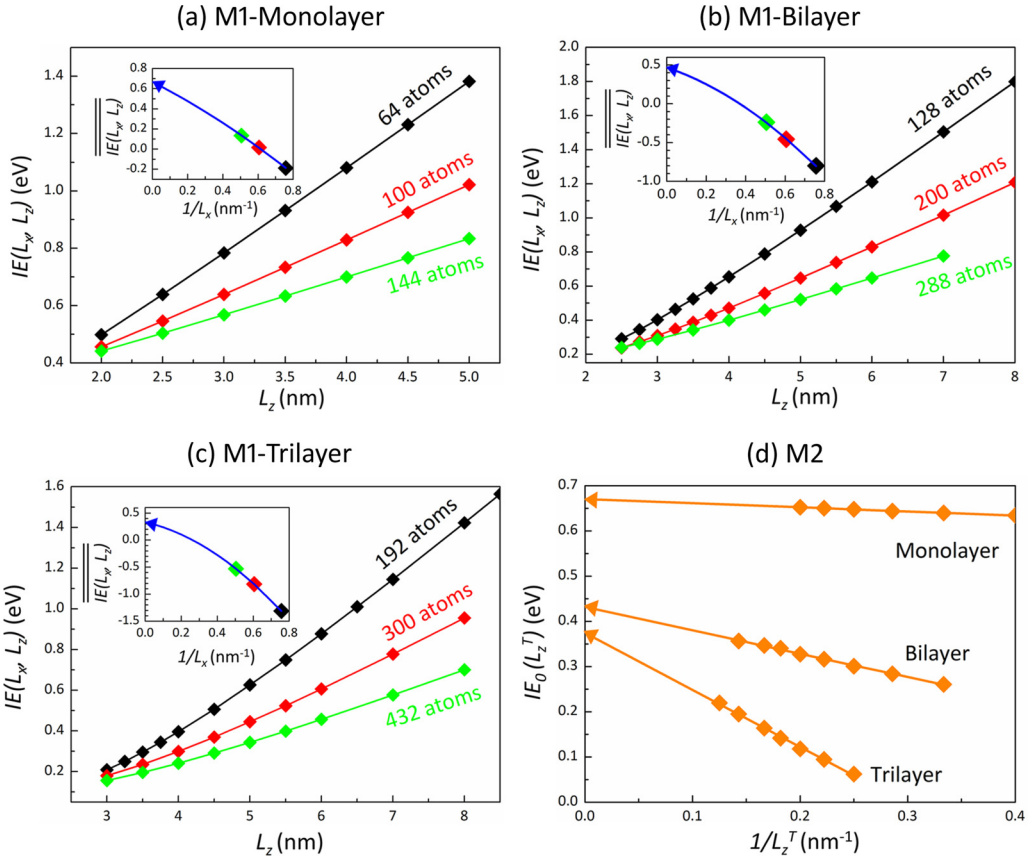

FIG. 3. (a)–(c) Method 1 (M1): Ionization energies of Te_P at different lateral dimensions (4×4, 5×5, and 6×6 for $L_x \times L_y$) as a function of L_Z in ML BP, 2L BP, and 3L BP, respectively. The insets show the value of $\overline{\overline{IE(L_x, L_Z)}} = \frac{c_{-2,0}}{L_x^2} + \frac{c_{-1,0}}{L_x} + IE_0$ as a function of $1/L_x$. The actual ionization energy IE_0s are indicated by blue arrows. (d) Method 2 (M2): $IE_0(L_Z^T)$ of Te_P as a function of $1/L_Z^T$ (L_Z^T, the threshold at which the terms of L_Z^{-2} and L_Z^{-1} are ignored) in ML BP, 2L BP, and 3L BP, respectively. The real ionization energy IE_0s are indicated by orange arrows. M1 and M2 mean that ionization energies are calculated with method 1 [Eq. (9)] and method 2 [Eq. (11)], respectively.

are well consistent with that obtained with method 1. Note that the decreasing ionization energies are not only a result of the up/down shifts of the VBM/CBM, but also a result of weakened Coulomb attraction due to increased dielectric screening. Although both methods perform well, the first one needs more calculation resources than the second one since the latter only requires the calculation of three or four points for the linear extrapolation. Moreover, the slope of the linear dependence is extremely small for thin films and becomes larger with increasing thickness. This means that the value of $IE_0(L_Z^T) - IE_0(L_Z^{T'})$ is minimal for the thinnest limitation. Figure 3 (d) shows that indeed this is the case for monolayer here where the energy difference between $IE_0(L_Z^T = 2.5\,\text{nm})$ and $IE_0(L_Z^{T'} \to \infty)$ is less than 0.04 eV. Therefore, sensible results can be obtained for monolayer at one appropriate L_Z^T without the need for linear extrapolation.

The thickness-dependent IE_0 is consistent with the calculated defect/impurity charge distributions, shown in Figs. 4(a)–4(c) along the in-plane (X and Y) and out-of-plane (Z) directions, for example, for Te_P. They show consistently that, with an increasing layer thickness, the spatial charge distributions of the gap states induced by the substitutional Te become more delocalized. One can see this from the in-plane charge distribution in Figs. 4(a)–4(b) where there is a significant reduction at the Te site especially between the ML and the 2L. Likewise, there is also a significant increase at the tail region away from Te. Although the increase may look small, taking into account the geometric factor of R^2, where R is the distance to Te indicates that the effect should be on par with that in the center since the total number of electrons for each state is conserved. One can also see this from the out-of-plane charge distribution in Fig. 4(c) where the tail extends into the second layer noticeably for the 2L and the 3L but not for the ML. One also can see a similar but less dramatic effect in the charge contour plot in Fig. 4(d). It appears that, in terms of the charge distribution, the most significant effect is between the ML and the 2L, which is consistent with the decreasing tendency of ionization energy.

To summarize, although Ref. [13] laid the foundation for first-principles determination of charged defects in monolayer 2D materials using the standard *jellium* background approximation, it requires a generalization of the approach to cases which are mostly used in the practical electronic devices, i.e., few/multilayer 2D semiconductors instead of monolayer, a layer of 2D material on a substrate, and surfaces/interfaces. It also requires a generalization to systems of arbitrary geometry and hence with less of a symmetry requirement in the method. These are carried out here. The method here is general

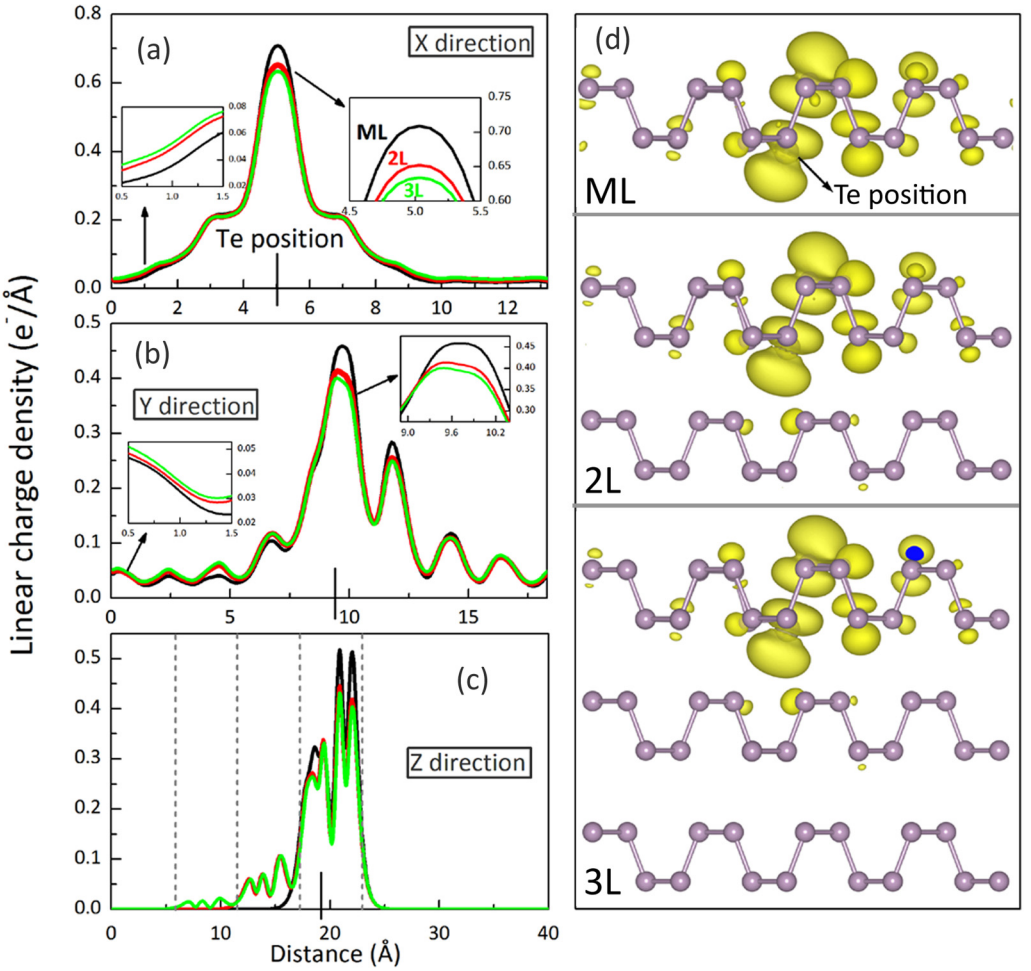

FIG. 4. Nonaveraged linear charge density (passing Te_P) along the in-plane (a) X, (b) Y, and (c) out-of-plane Z directions in ML BP, 2L BP, and 3L BP, respectively. The vertical solid line marks the position of the Te impurity. The dotted lines in (c) denote the physical boundary of each P layer. (d) Charge contour plots with an isosurface of $8 \times 10^{-4}\, e/\text{Å}^3$.

and suitable for all 2D materials with arbitrary thickness and geometry. With the generalized approach, the dopability of 2D and quasi-2D materials, which is crucial for their application in electronic and optoelectronic devices, can be evaluated by the calculation of ionization energy. Application to black phosphorus, in particular, to substitutional Te (Te_P, the most promising candidate for n-type doping) in few-layer BP reveals that enhanced screening indeed exists and can reduce the Coulomb attraction between opposite charges to result in the dopant wave-function delocalization as well as shallower levels. The ionization energy of Te_P decreases by nearly half in 3L BP (0.33 eV) in comparison with that in ML BP (0.67 eV). These results further suggest that, for 2D applications, single-layer materials may not always be the best choice, but few-layer materials can offer the most balanced properties for novel electronic and optoelectronic applications.

ACKNOWLEDGMENTS

Work in China was supported by the National Natural Science Foundation of China and The National Key Research and Development Program of China under Grants No. 11374119, No. 61590930, No. 2017YFB1104300, No. 91423102, No. 2014CB921303, and No. 11504368. Work at RPI was supported by the Department of Energy under Grant No. DE-SC0002623. Also, we acknowledge the High-Performance Computing Center (HPCC) at Jilin University for calculation resources. Professor X.-B. Li sincerely thanks Professor S. Zhang and Professor H.-B. Sun for their 10-year support for the laboratory of *Computational Semiconductor Physics* at JLU [38].

APPENDIX: CALCULATION OF $\varepsilon_\perp$ FOR THE 2D MATERIAL WITH A CERTAIN THICKNESS

The calculated dielectric constant in VASP for a supercell with L_Z can be approximated by an average of the dielectric constant for the 2D material with thickness of $2d_0(\varepsilon_\perp)$ and that for the vacuum region (with a thickness of $L_Z - 2d_0$) [16], namely,

$$\varepsilon_\perp^{\text{ave}} = \frac{2d_0\varepsilon_\perp + (L_Z - 2d_0) \times 1}{L_Z}.$$

Here, $\varepsilon_\perp$ is the relative dielectric constant we needed for the 2D material (the vertical scope from the top atom to the bottom atom), and the relative dielectric constant of vacuum

is 1. The expression can change to

$$\varepsilon_{\perp}^{\text{ave}} = \frac{2d_0\varepsilon_{\perp} + (L_Z - 2d_0)}{L_Z} = 1 + \frac{1}{L_Z}[2d_0(\varepsilon_{\perp} - 1)] = 1 + \frac{1}{L_Z}k.$$

As such, $\varepsilon_{\perp}^{\text{ave}}$ is inversely proportional to L_Z with a slope k. We can get $\varepsilon_{\perp}$ via the fitting slope k, i.e., $\varepsilon_{\perp} = 1 + \frac{k}{2d_0}$.

[1] B. Radisavljevic, A. Radenovic, J. Brivio, V. Giacometti, and A. Kis, Nat. Nanotechnol. **6**, 147 (2011).
[2] Q. H. Wang, K. Kalantar-Zadeh, A. Kis, J. N. Coleman, and M. S. Strano, Nat. Nanotechnol. **7**, 699 (2012).
[3] M. Xu, T. Liang, M. Shi, and H. Chen, Chem. Rev. **113**, 3766 (2013).
[4] H. Liu, A. T. Neal, Z. Zhu, Z. Luo, X. Xu, D. Tománek, and P. D. Ye, ACS Nano **8**, 4033 (2014).
[5] L. Li, Y. Yu, G. J. Ye, Q. Ge, X. Ou, H. Wu, D. Feng, X. H. Chen, and Y. Zhang, Nat. Nanotechnol. **9**, 372 (2014).
[6] J. Qiao, X. Kong, Z.-X. Hu, F. Yang, and W. Ji, Nat. Commun. **5**, 4475 (2014).
[7] J. Yang, R. Xu, J. Pei, Y. W. Myint, F. Wang, Z. Wang, S. Zhang, Z. Yu, and Y. Lu, Light: Sci. Appl. **4**, e312 (2015).
[8] Y. Abate, S. Gamage, Z. Li, V. Babicheva, M. H. Javani, H. Wang, S. B. Cronin, and M. I. Stockman, Light: Sci. Appl. **5**, e16162 (2016).
[9] S. B. Zhang, J. Phys.: Condens. Matter **14**, R881 (2002).
[10] C. G. Van de Walle, J. Appl. Phys. **95**, 3851 (2004).
[11] S.-H. Wei, Comput. Mater. Sci. **30**, 337 (2004).
[12] C. Freysoldt, B. Grabowski, T. Hickel, J. Neugebauer, G. Kresse, A. Janotti, and C. G. Van de Walle, Rev. Mod. Phys. **86**, 253 (2014).
[13] D. Wang, D. Han, X.-B. Li, S.-Y. Xie, N.-K. Chen, W. Q. Tian, D. West, H.-B. Sun, and S. B. Zhang, Phys. Rev. Lett. **114**, 196801 (2015).
[14] H.-P. Komsa and A. Pasquarello, Phys. Rev. Lett. **110**, 095505 (2013).
[15] J.-Y. Noh, H. Kim, M. Park, and Y.-S. Kim, Phys. Rev. B **92**, 115431 (2015).
[16] J.-Y. Noh, H. Kim, and Y.-S. Kim, Phys. Rev. B **89**, 205417 (2014).
[17] H. Liu, A. T. Neal, M. Si, Y. Du, and P. D. Ye, IEEE Electron Device Lett. **35**, 795 (2014).
[18] N. R. Pradhan, D. Rhodes, S. Feng, Y. Xin, S. Memaran, B.-H. Moon, H. Terrones, M. Terrones, and L. Balicas, ACS Nano **8**, 5911 (2014).
[19] T. Kanazawa, T. Amemiya, A. Ishikawa, V. Upadhyaya, K. Tsuruta, T. Tanaka, and Y. Miyamoto, Sci. Rep. **6**, 22277 (2016).
[20] M. W. Lin, I. I. Kravchenko, J. Fowlkes, X. Li, A. A. Puretzky, C. M. Rouleau, D. B. Geohegan, and K. Xiao, Nanotechnology **27**, 165203 (2016).
[21] T. Pei, L. Bao, G. Wang, R. Ma, H. Yang, J. Li, C. Gu, S. Pantelides, S. Du, and H.-j. Gao, Appl. Phys. Lett. **108**, 053506 (2016).
[22] S. B. Desai, S. R. Madhvapathy, A. B. Sachid, J. P. Llinas, Q. Wang, G. H. Ahn, G. Pitner, M. J. Kim, J. Bokor, C. Hu, H.-S. Philip Wong, and A. Javey, Science **354**, 99 (2016).
[23] P. Hohenberg and W. Kohn, Phys. Rev. **136**, B864 (1964).
[24] W. Kohn and L. J. Sham, Phys. Rev. **140**, A1133 (1965).
[25] J. P. Perdew, K. Burke, and M. Ernzerhof, Phys. Rev. Lett. **77**, 3865 (1996).
[26] G. Kresse and J. Furthmüller, Phys. Rev. B **54**, 11169 (1996).
[27] G. Kresse and J. Furthmüller, Comput. Mater. Sci. **6**, 15 (1996).
[28] J. Paier, M. Marsman, K. Hummer, G. Kresse, I. C. Gerber, and J. G. Angyan, J. Chem. Phys. **124**, 154709 (2006).
[29] E. N. Brothers, A. F. Izmaylov, J. O. Normand, V. Barone, and G. E. Scuseria, J. Chem. Phys. **129**, 011102 (2008).
[30] C. G. Van de Walle, P. J. H. Denteneer, Y. Bar-Yam, and S. T. Pantelides, Phys. Rev. B **39**, 10791 (1989).
[31] J. Lento, J.-L. Mozos, and R. M. Nieminen, J. Phys.: Condens. Matter **14**, 2637 (2002).
[32] S. B. Zhang and J. E. Northrup, Phys. Rev. Lett. **67**, 2339 (1991).
[33] S. Das, W. Zhang, M. Demarteau, A. Hoffmann, M. Dubey, and A. Roelofs, Nano Lett. **14**, 5733 (2014).
[34] Y. Deng, Z. Luo, N. J. Conrad, H. Liu, Y. Gong, S. Najmaei, P. M. Ajayan, J. Lou, X. Xu, and P. D. Ye, ACS Nano **8**, 8292 (2014).
[35] H. Yuan, X. Liu, F. Afshinmanesh, W. Li, G. Xu, J. Sun, B. Lian, A. G. Curto, G. Ye, Y. Hikita, Z. Shen, S. C. Zhang, X. Chen, M. Brongersma, H. Y. Hwang, and Y. Cui, Nat. Nanotechnol. **10**, 707 (2015).
[36] D. West, Y. Y. Sun, and S. B. Zhang, Appl. Phys. Lett. **101**, 082105 (2012).
[37] W. Chen and A. Pasquarello, J. Phys.: Condens. Matter **27**, 133202 (2015).
[38] http://www.ioe-jlu.cn/csp.